RSC Advances

PAPER

View Article Online
View Journal | View Issue

Check for updates

Cite this: *RSC Adv.*, 2023, **13**, 2010

A molecular dynamics study on adsorption mechanisms of polar, cationic, and anionic polymers on montmorillonite†

Yuanzhi Qu,‡[a] Ling Lin,‡[b] Shifeng Gao,[a] Yukun Yang,[b] Hongjun Huang,[a] Xin Li,[b] Han Ren[a] and Wenjia Luo*[b]

Adsorption of polymers on clay in aqueous solutions has wide applications in environmental, medical, and energy-related areas, but the interactions between polymers and clay under varied conditions are still not fully understood. In this study, we investigated the adsorption mechanisms of four polymers belonging to different categories, namely anionic poly(acrylic acid) (poly-AA), cationic poly(diallyldimethylammonium chloride) (poly-DADMAC), nonionic polyacrylamide (poly-AM), and the copolymer of AA and DADMAC (poly-AADADMAC). By using molecular dynamics simulations, we compared the desorption kinetics of these polymers at different temperatures and found that poly-AA and poly-AM have the weakest and strongest adsorption abilities, respectively. Polymer adsorptions are slightly more stable at higher pressures, and high salinity favors the adsorption of charged polymers. Further analysis suggests that the adsorption of anionic poly-AA is less stable than that of cationic poly-DADMAC because the latter is attracted to the negatively charged surface by direct coulombic forces, and poly-AM is stabilized by van der Waals forces and hydrogen bonds. This study provides insights on how to enhance the adsorption affinity of polymers on a clay surface and may help the design or improvement of polymer/clay nanocomposite materials.

Received 18th November 2022
Accepted 12th December 2022

DOI: 10.1039/d2ra07341b

rsc.li/rsc-advances

Open Access Article. Published on 11 January 2023. Downloaded on 12/19/2025 10:25:52 PM.
This article is licensed under a Creative Commons Attribution-NonCommercial 3.0 Unported Licence.

1 Introduction

Polymer-clay nanocomposite (PCNC) materials are widely used in multiple areas, for example as adsorbents of pollutants in wastewater treatment[1–4] or as drug delivery systems in medical applications.[5,6] PCNC materials have particularly important applications in oil and gas drilling operations, where they are often used as multipurpose additives of drilling fluids. The roles of PCNCs include but are not limited to improving rheological properties of drilling fluid,[7,8] preventing fluid loss,[9,10] elevating carrying capacity, inhibiting the hydration and swelling of shale,[11–14] and conducting heat.[10]

PCNC materials are prepared by combining polymers with clay minerals. Currently, there are two major approaches to preparing PCNC materials, which are chemical grafting and physical adsorption.[15] In the former approach, clay surfaces are modified chemically and the polymers are linked to the clay surface *via* covalent bonds.[16–19] On the other hand, polymers can also be physically adsorbed on clay *via* van der Waal, electrostatic, and hydrogen-bonding interactions.[20–23] Our aim in this study is to investigate the general principles behind polymer/clay interactions, but the strength of chemisorption depends on the number and distributions of chemical bonds, which are determined by the specific preparation method and cannot be discussed unless the details of preparation method are provided. Therefore, we focus only on physical adsorption in this paper.

Understanding the interaction between polymer and clay is the key to improving the design and application of novel PCNC materials that can have satisfactory performance under certain working conditions. For example, additives of drilling fluids must withstand high temperatures (>400 K), high pressures (>100 MPa), and high salinity conditions (up to saturation) in deep wellbores.[24–26] Polymer adsorption on clay minerals can be investigated by various experimental techniques, including Fourier transform infrared spectroscopy (FTIR), X-ray diffraction (XRD), atomic force microscopy (AFM), ζ potential, particle size distribution, to measure adsorption amount, adsorption site, polymer conformation, mechanical strength, clay basal spacing, and many other quantities.[27–29] Such results can be analyzed to provide insights into the adsorption mechanisms. For example, Nakatani *et al.* studied the effect of polymer conformation,[30] Kohay *et al.* investigated the influence of polycation density,[31] Sengwa *et al.* compared polymers with different

[a]*CNPC Engineering Technology R&D Company Limited, Beijing, 102206, P. R. China*
[b]*School of Chemistry and Chemical Engineering, Southwest Petroleum University, Chengdu, 610500, P. R. China. E-mail: luowenjia@swpu.edu.cn*

† Electronic supplementary information (ESI) available. See DOI: https://doi.org/10.1039/d2ra07341b

‡ Yuanzhi Qu and Ling Lin contributed equally to this work.

© 2023 The Author(s). Published by the Royal Society of Chemistry

Open Access Article. Published on 11 January 2023. Downloaded on 12/19/2025 10:25:52 PM.
This article is licensed under a Creative Commons Attribution-NonCommercial 3.0 Unported Licence.

structures,[32] and Kádár *et al.* focused on clay surface characteristics.[27]

Although experimental techniques are versatile, quantizable, and indispensable in the research of PCNC materials, it is usually challenging to experimentally investigate the microscopic adsorption mechanisms at the molecular level. Instead, molecular dynamics (MD) and related computational methods can be used to simulate the adsorption process of polymers and predict the properties of PCNC materials. Reviews by Pereira *et al.*,[33] Suter *et al.*,[34] Cygan *et al.*,[35] and Teppen *et al.*[36] summarized early attempts to study clay materials by MD and numerical simulations. Camara *et al.*,[37] Greathouse *et al.*,[38] Shahriyari *et al.*,[39] and Yang *et al.*[40] simulated the adsorption of salts on clay, while many other researchers focused on the adsorption of organic or inorganic small molecules on clay.[41–45] Wang *et al.*[46] studied the wettability of silica, and Yu *et al.*[47] investigated the phase equilibrium of *n*-pentane in quartz pores. The formation mechanisms of CO_2 hydrate[48,49] or CH_4 hydrate[50,51] in pores of various types of clay minerals were examined using molecular simulation methods, and the effect of cations was discussed.[51]

The adsorption of various kinds of polymers on clay have been investigated, which include but are not limited to bitumen,[52] poly(butylene 2,5-furan-dicarboxylate),[53] poly(lactic-co-glycolic acid),[54] chitin and chitosan,[55] xyloglucans,[56,57] poly(ethylene glycol),[58,59] poly(ε-caprolactone),[60,61] and poly(ethylene oxide).[62] While most researchers chose montmorillonite (MMT) to represent clay, some other studies considered other types of clay including quartz,[63] kaolinite,[64] and silica.[65]

In many studies, the authors focused on predicting the mechanical,[66–68] rheological,[69,70] or thermodynamical properties[71,72] of the PCNC materials. On the other hand, many other researchers investigated the adsorption mechanisms of polymers and provided insights on how to enhance the adsorption. For example, Sun *et al.* demonstrated that divalent Ca^{2+} ions can enhance the adsorption of anionic polymers,[73] and cationic chitosan can enhance the adsorption of neutral poly(acrylamide).[74] Quezada showed that the adsorption strength of hydrolyzed polyacrylamide is proportional to salinity but inversely proportional to surface charge concentration.[63] Jamil *et al.* suggested that ionic clouds formed on the basal plane of clay can enhance the adsorption of polymers.[75] Haouti *et al.* compared the adsorption strengths of two cationic molecules on clay.[76] Experimental studies on the effects of temperatures, pressures, and salinity on polymer adsorption are widely available. For example, Mpofu *et al.* showed that temperatures up to 90 °C and salt concentrations up to 0.01 M have limited effect on polyetheramine adsorption on MMT.[77] Tekin *et al.* investigated the adsorption of cationic polyacrylamide onto sepiolite under temperatures up to 55 °C.[78] However, to the best of our knowledge, few molecular dynamics studies have been reported on comparing the adsorption mechanisms of different types of polymers on clay, especially the desorption under high temperatures.

In this study, we aim to compare the adsorption mechanisms of different types of polymers on MMT. Poly(acrylic acid) (poly-AA), poly(diallyldimethylammonium chloride) (poly-DADMAC), and polyacrylamide (poly-AM). We chose these polymers both because they are widely used in drilling fluids and also because each of them represents a different category of polymers. Specifically, poly-AA, poly-DADMAC, and poly-AM represent anionic, cation, and nonionic polymers. In addition, the copolymer of acrylic acid and diallyldimethylammonium chloride (poly-AADADMAC) was selected to represent polymers that possess both positive and negative charges. In Section 2 we describe how the molecular system was constructed and the forcefield used in this study. In Section 3 we compare the desorption kinetics of these polymers under different temperatures and investigate the conditions that can affect the adsorption stability such as salinity and pressure. Finally, we provide insights on how to enhance the adsorption affinity based on the simulation results.

2 Methods

2.1 The molecular model

We chose a classical Na-montmorillonite (Na-MMT) model ($Na_3(Si_{31}Al)(Al_{14}Mg_2)O_{80}(OH)_{16}\cdot nH_2O$) to represent the typical composition of a sodium smectite clay.[79,80] In this model, one Al^{3+} and two Mg^{2+} ions replace one octahedral Si^{4+} and two octahedral Al^{3+} ions, leaving the MMT layer carrying three negative charges. The size of this model is 1.036 nm × 1.796 nm in the *x* and *y* directions. To simulate the adsorption of polymers on a large clay surface, we created a 10 × 5 supercell, which is 10.36 nm × 8.98 nm wide, to represent one MMT layer.

Our computational model is shown in Fig. 1. In this model, two identical MMT plates were placed in the *xy*-plane and separated by around 6.0 nm, and the lower plate was designated to be the adsorption site for polymers. This 6.0 nm layer-to-layer distance corresponds to an inter-layer spacing of around 6.6 nm. Although experimentally measured basal spacing of MMT intercalated by polymers is usually less than 5 nm,[17] we found that this 5 nm spacing is too narrow to simulate the complete desorption of polymers into the solution; the polymer must be at least 3.0 nm away from both plates. On the other hand, using an even larger spacing would dramatically increase the demand on computational resources and is unnecessary.

As stated in the Introduction section, we considered four types of polymers, poly-AA, poly-DADMAC, poly-AADADMAC, and poly-AM, in this study. At the start of each simulation, nine identical polymer chains were placed above the lower plate in a 3-by-3 fashion as shown in Fig. 1. By adjusting the number of repeating units, chains of different polymers have similar lengths of around 2 nm. Parameters of polymer chains including the numbers of atoms and molecular weights are summarized in Table 1. The structures of these four polymer chains are further illustrated in Fig. S1.†

Counter ions, K^+ or Cl^-, were added to the system where the anionic poly-AA or the cationic poly-DADMAC are present to always keep the system charge-neutral. The space between the upper and lower plates was filled with water and salt (10 wt% KCl, unless otherwise stated), where the percent by weight (wt%) means the mass of salt divided by the mass of the salt solution (excluding polymer and clay). And the 10 wt% KCl

Open Access Article. Published on 11 January 2023. Downloaded on 12/19/2025 10:25:52 PM.
This article is licensed under a Creative Commons Attribution-NonCommercial 3.0 Unported Licence.

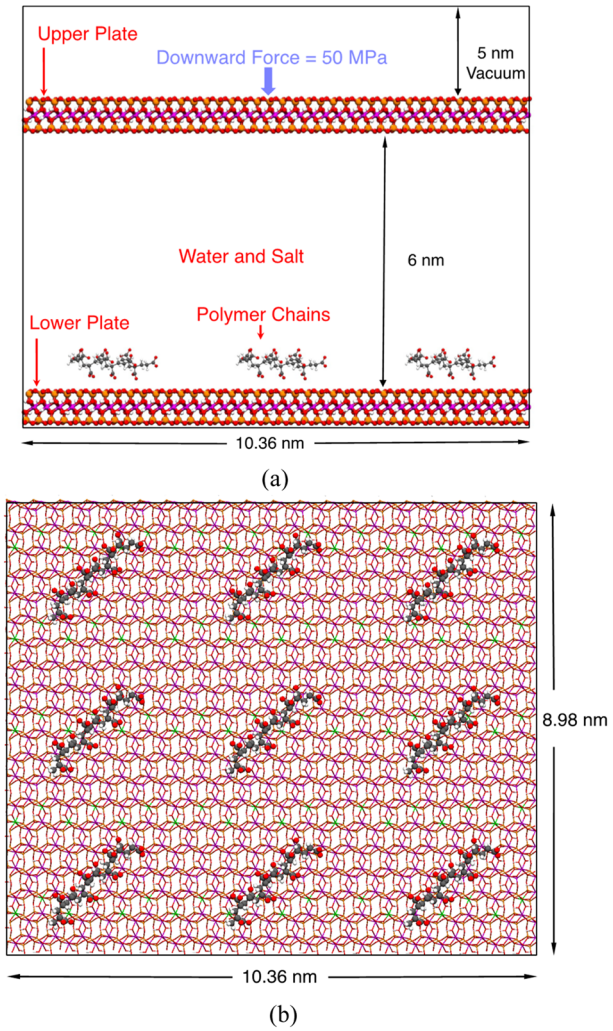

Fig. 1 Front (a) and top (b) views of the molecular model in this study. The black boxes outline the boundaries of a periodic unit cell. Red, orange, magenta, green, white, and gray spheres represent O, Si, Al, Mg, H, and C atoms, respectively. This figure shows, as an example, poly-AA chains adsorbed on the MMT surface. The space between the upper and lower plates is filled with water and salt, which are not shown in this figure for clarity. The upper plate is also hidden in the top view to make the polymers visible.

concentration is equivalent to a mole fraction of 0.026. A periodic boundary condition was imposed on the simulation box and a vacuum space of at least 5.0 nm was left between periodic images in the z-direction. In all simulations, the lower plate was fixed in space, while the upper plate is mobile and experienced a constant downward force equivalent to a pressure of 50 MPa unless otherwise stated. Therefore, all simulations in this study were effectively performed under constant-pressure conditions although the volume of the simulation box was fixed. To simplify the problem, we did not consider the influence of pH values by adding additional H^+ or OH^- ions. In other words, all calculations were performed at a constant pH value of 7.

2.2 Molecular dynamics

All molecular dynamics (MD) simulations were performed using the LAMMPS program.[81] Pairwise interactions and atomic charges were described by a combination of forcefields. Specifically, the MMT layers and ions were described by the CLAYFF forcefield.[79] The MD parameters of polymers, including bonded and non-bonded interactions, were taken from the OPLS all-atom forcefield (OPLS-AA).[82] Water molecules were described by the SPC/E model of Berendsen *et al.*[83] For all nonbonded interactions, the van der Waals and electrostatic forces as given by eqn (1) were considered.

$$E_{ab} = \sum_{i}^{on\ a} \sum_{j}^{on\ b} \left[\frac{q_i q_j e^2}{r_{ij}} + 4\varepsilon_{ij} \left(\frac{\sigma_{ij}^{12}}{r_{ij}^{12}} - \frac{\sigma_{ij}^{6}}{r_{ij}^{6}} \right) \right] \quad (1)$$

Mixing rules are used for van der Waals parameters of unlike atoms by eqn (2)

$$\varepsilon_{ij} = \sqrt{\varepsilon_i \varepsilon_j}\ ,\ \sigma_{ij} = \frac{\sigma_i + \sigma_j}{2} \quad (2)$$

Long-range electrostatic interactions were summed by using the particle–particle particle-mesh (PPPM) method with an accuracy of 10^{-4}.[84] As explained in Section 2.1, although all simulations were performed under constant pressure conditions because of the external forces applied on the upper plate, the volume and shape of the periodic simulation box were fixed, therefore the MD runs were under the NVT ensemble with a Nosé–Hoover thermostat.[85] All simulations were performed with a time step of 1.0 fs and a total integration time of 5.0 ns. Moreover, each simulation has been repeated three times by starting from different random velocities, and the averaged results of three independent runs were reported.

Self-diffusion coefficients (D_s) were estimated from the mean-squared displacement (MSD) based on the Einstein

Table 1 Parameters of four polymers modeled in this study

Polymer	Repeating units[a]	Number of atoms[b]	Molecular weight	Charge
Poly-AA	10	82	712.57	−10.0
Poly-DADMAC	6	152	759.35	6.0
Poly-AADADMAC[c]	10	167	988.41	0.0
Poly-AM	10	102	712.81	0.0

[a] All chains are isotactic. [b] Excluding counter ions for poly-AA and poly-DADMAC. [c] Poly-AADADMAC is an alternating copolymer consisting of five AA and five DADMAC units. Each AA and DADMAC unit carry a negative and positive charge, respectively.

© 2023 The Author(s). Published by the Royal Society of Chemistry

Open Access Article. Published on 11 January 2023. Downloaded on 12/19/2025 10:25:52 PM.
This article is licensed under a Creative Commons Attribution-NonCommercial 3.0 Unported Licence.

model (eqn (3)), where N is the number of total atoms and $r_k(t)$ is the position of atom k at time t.

$$D_s = \lim_{t\to\infty} \frac{1}{6tN} \sum_{k=1}^{N} |r_k(t) - r_k(0)|^2 \quad (3)$$

3 Results and discussion

3.1 Polymer desorption under different conditions

In this section, we report the MD simulation results of polymer desorption from the MMT surface. Specifically, we compare the desorption behaviors of four polymers and consider the influence of temperatures, pressures, salinity, and salt types.

3.1.1 Temperatures. For each polymer, we created an initial structure in which nine identical chains were placed above the MMT surface. For example, Fig. 1 shows the initial structure for poly-AA chains adsorbed on MMT. Starting from each initial structure, energy minimization was performed followed by a 5 ns MD run to investigate how the polymer chains desorb from the surface. Firstly, we calculated the distances from the centers of polymer chains to the MMT surface, and the averaged polymer/surface distances are plotted in Fig. 2 as curves. Secondly, we calculated the ratio of adsorbed chains at each time step by considering a chain as adsorbed if its minimum distance from the surface is less than 0.4 nm and desorbed if otherwise. We take 0.4 nm as the threshold because the sum of van der Waals radii of most atom pairs involved in this study is less than 0.4 nm. Although this particular threshold is rather arbitrary, all adsorption ratios would increase or decrease uniformly if a larger or smaller threshold was used, leaving the overall trend unaltered. The percentages of adsorbed chains are further time-averaged over each quarter nanosecond and are shown as bars in Fig. 2.

Fig. 2 shows averaged results of three independent runs. We have further provided the results of each separate run in ESI Fig. S2,† which also includes the simulations under an even lower temperature (275 K).

Both the polymer/MMT distances and adsorption percentages indicate that the adsorption of all polymers becomes less stable under higher temperatures.

As shown in Fig. 2(a), the adsorption of poly-AA is the least stable among all four polymers. Even at room temperatures (300 K), poly-AA chains steadily desorb from the surface and are on average 1.5 nm above the surface at 5.0 ns. Under higher temperatures (400–500 K), poly-AA chains desorb even faster with adsorption rates dropping to nearly zero after 3.0 ns.

The adsorption of poly-AADADMAC (Fig. 2(c)) is more stable than poly-AA (Fig. 2(a)) but less stable than poly-DADMAC (Fig. 2(b)). Poly-DADMAC can retain nearly 40% adsorption ratio at 500 K after 5 ns, while for poly-AADADMAC only 15% of chains remain on the surface under the same conditions.

Surprisingly, poly-AM shows exceptional adsorption stability as shown in Fig. 2(d). Its adsorption is completely stable at 300 K and 400 K. Only in the highest temperature (500 K), poly-AM slightly desorbs from the surface but its adsorption rate never drops below 75%. While the adsorption mechanism of poly-AA, which is presumably different from those of the other three polymers, will be further investigated in the subsequent sections, at this point we can qualitatively conclude that the relative adsorption stability of these four polymers follows the order of poly-AM > poly-DADMAC > poly-AADADMAC > poly-AA.

This order of adsorption stability loosely matches the order of self-diffusion coefficients (D_s) of polymers listed in Table 2 at least for temperatures below 400 K. For example, the D_s of poly-AA are two to five times higher than that of poly-AM. A more detailed table containing D_s values of water and salt ions is provided as Table S1.†

3.1.2 Pressures. All simulations in Section 3.1.1 were performed at 50 MPa. We also tested the influence of applied pressures. Desorption behaviors of four polymers at 400 K and different pressures (20 MPa, 50 MPa, 200 MPa) are shown in Fig. 3. The results at 50 MPa are previously displayed in Fig. 2 but are replicated here for comparison.

Based on Fig. 3, we conclude that pressures varying between 20 and 200 MPa have a weak influence on the desorption behaviors of polymers. Except for poly-AM, the other three polymers have slightly stronger adsorption under higher pressures. A possible reason is that the elevated density of the polymer/salt solution (approximately 1.01 g cm^{-3} at 20 MPa and 1.08 g cm^{-3} at 200 MPa, see Table S2†) under high pressures reduces the mobility of polymer chains by decreasing the D_s values of polymer chains and salt ions. For example, Table 3 suggests that the D_s of poly-AA decreases from 0.63 to 0.40 from 20 MPa to 200 MPa. Table S2† further lists the density of the polymer/salt solution and the D_s values of K^+, Cl^-, and water. Especially for water, its D_s strictly decreases as the pressure rises.

3.1.3 Salinity. Salinity may influence the adsorption stability of polymers. We compared the desorption of polymers under different salt (KCl) concentrations varying between 0 wt% and 20 wt%. The desorption rates of these four polymers at 500 K are shown in Fig. 4. In this figure, the results for 10 wt% KCl are previously shown in Fig. 2 and are replicated here for comparison. At this high temperature (500 K), all polymers except poly-AA will completely desorb into the aqueous phase after two to three nanoseconds. As a comparison, the desorption behaviors of polymers at a low temperature (275 K) were also examined and shown in Fig. S3.† D_s of salt ions, polymers, and water under different KCl concentrations are tabulated in Table S3.†

For poly-AA, Fig. 4(a) suggests that the adsorption rate is inversely proportional to the salinity, at least in the first two nanoseconds. With no salt at all, the polymer quickly detaches (distance > 3.0 nm) from the surface in just half a nanosecond, while when a high concentration of KCl (20 wt%) is present, the desorption process is significantly delayed. However, after the poly-AA chains fully desorb from the surface after 2 ns, both the adsorption rates and distances are no longer dependent on salinity.

Desorption of poly-DADMAC has a more profound dependence on salinity as depicted in Fig. 4(b). A high concentration of 20% KCl can significantly enhance the adsorption of poly-

Open Access Article. Published on 11 January 2023. Downloaded on 12/19/2025 10:25:52 PM.
This article is licensed under a Creative Commons Attribution-NonCommercial 3.0 Unported Licence.

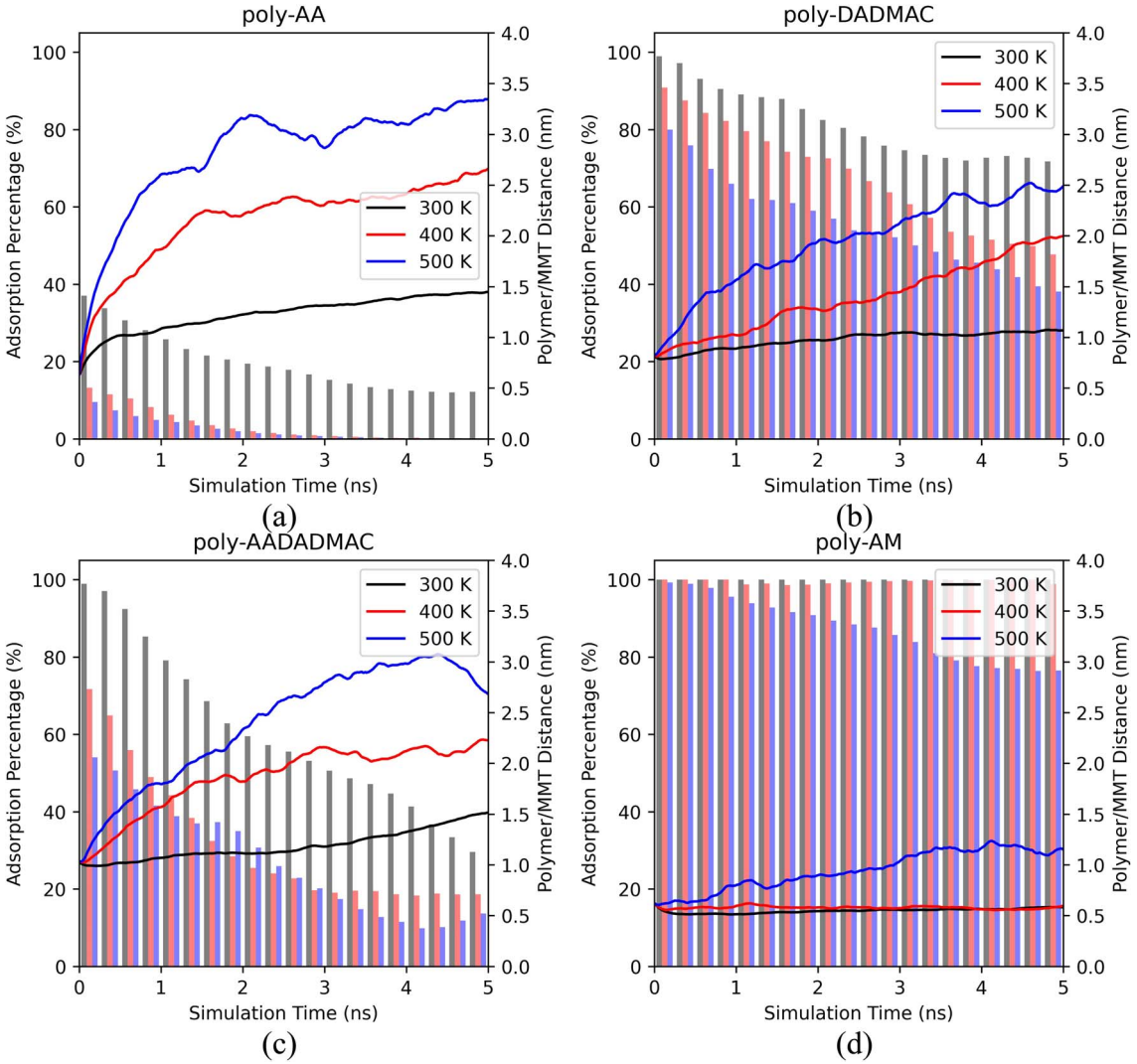

Fig. 2 The polymer/MMT distances (curves, axis on the right) and the ratios of adsorbed polymer chains (bars, axis on the left) of (a) poly-AA, (b) poly-DADMAC, (c) poly-AADADMAC, and (d) poly-AM as functions of MD simulation time under different temperatures. In the calculations of the polymer/MMT distances, the distance is measured from the center of the polymer chain to the MMT surface. In the calculations of adsorption percentages, a chain is considered to be adsorbed if its minimum distance to the surface is less than 0.4 nm. All simulations were at 50 MPa, in 10% wt KCl solution.

Table 2 D_s of four polymers on MMT at different temperatures[a]

	D_s (10^{-9} m^2 s^{-1})		
Polymer	300 K	400 K	500 K
Poly-AA	0.1014	0.5059	2.4269
Poly-DADMAC	0.0513	0.4728	1.2065
Poly-AADADMAC	0.0615	0.4678	0.8268
Poly-AM	0.0233	0.1264	0.9311

[a] All simulations in this table are at 50 MPa, in 10 wt% KCl solution.

DADMAC within the entire simulated time range. However, there is no obvious difference in adsorption ratios among 0%, 5%, and 10% concentrations.

For poly-AADADMAC and poly-AM shown in Fig. 4(c) and (d), salinity has a less obvious influence on the desorption rates. In the first nanosecond, desorption rates under different salinity are almost the same (difference in desorption distance <0.5 nm). At a longer timescale (2–5 ns), the desorption distances and adsorption rates show no correlation with the salinity and are more likely a consequence of random distribution due to the Brownian motion of partially desorbed polymer chains.

Therefore, we conclude that high salinity (≥20%) can enhance the adsorption of poly-AA and poly-DADMAC, which are both charged polymers. On the other hand, salinity has no apparent influence on the desorption rates of poly-AADADMAC and poly-AM. For poly-AA, a high salinity may slow down, but not prevent its desorption at high temperatures (500 K).

3.1.4 Salt types. Recently, Sun *et al.* found that divalent cations can enhance the adsorption of anionic polyacrylamide

© 2023 The Author(s). Published by the Royal Society of Chemistry

Open Access Article. Published on 11 January 2023. Downloaded on 12/19/2025 10:25:52 PM.
This article is licensed under a Creative Commons Attribution-NonCommercial 3.0 Unported Licence.

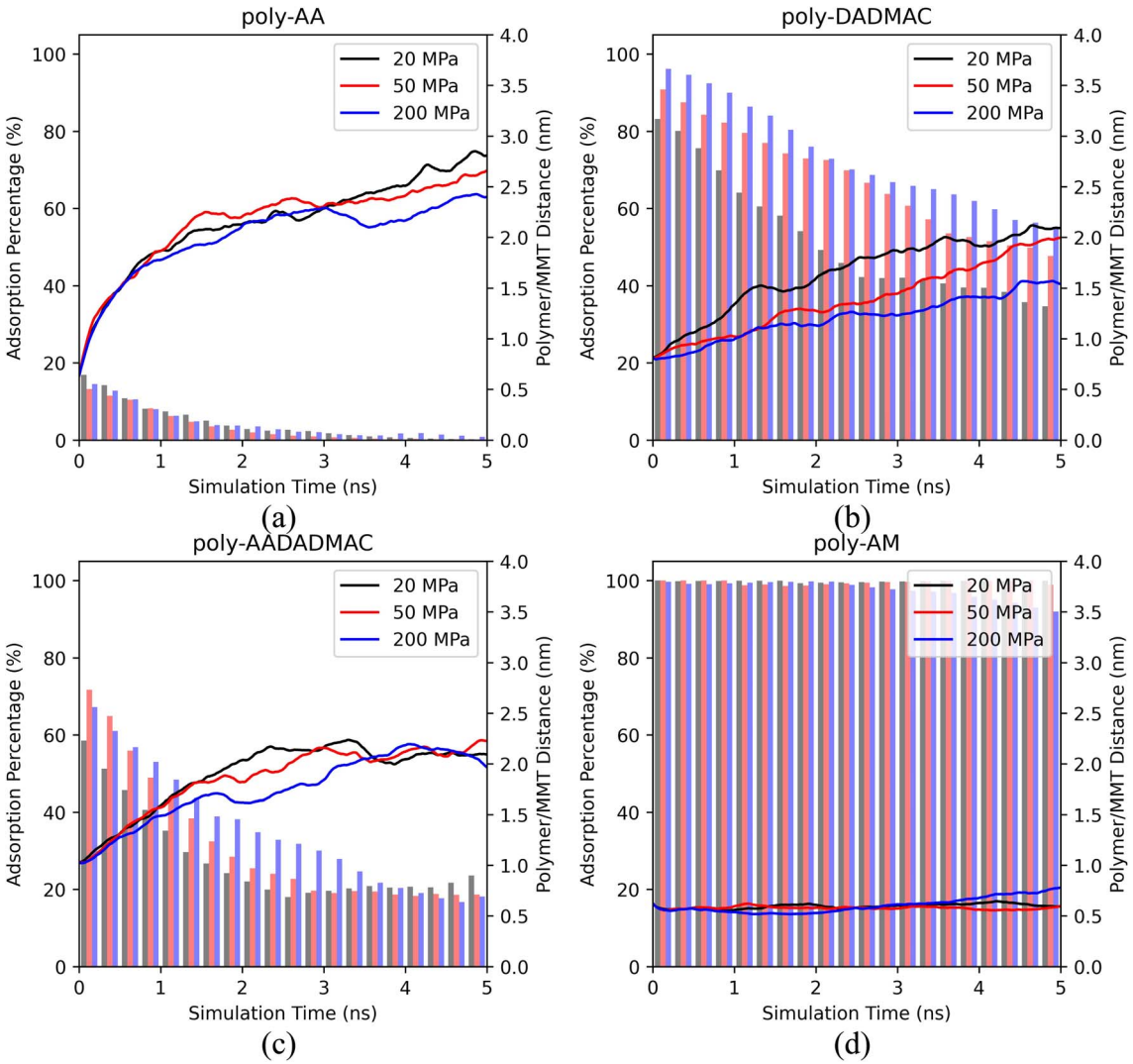

Fig. 3 The polymer/MMT distances and the ratios of adsorbed polymer chains of (a) poly-AA, (b) poly-DADMAC, (c) poly-AADADMAC, and (d) poly-AM as functions of MD simulation time under different pressures. All simulations were at 400 K, in 10 wt% KCl solution.

Table 3 D_s of four polymers on MMT under different pressures[a]

	D_s (10^{-9} m^2 s^{-1})		
Polymer	20 MPa	50 MPa	200 MPa
Poly-AA	0.6325	0.5059	0.4014
Poly-DADMAC	0.5737	0.4728	0.4382
Poly-AADADMAC	0.5182	0.4678	0.5069
Poly-AM	0.2010	0.1264	0.1563

[a] All simulations in this table are at 400 K, in 10 wt% KCl solution.

(a copolymer of acrylic acid and acrylamide) on MMT through molecular dynamics simulations.[73] We performed similar studies and compared the desorption rate of poly-AA under 10.0 wt% KCl and 7.54 wt% $CaCl_2$. This specific $CaCl_2$ concentration (7.54 wt%) was chosen to make the molar ratios of Cl^- equal to 0.026 in both cases (the number of Ca^{2+} equals half of K^+), therefore a fair comparison between these two cations can be made. Fig. 5 compares the desorption of four polymers at 500 K. Additional comparisons at the low temperature (275 K) are provided in Fig. S4.†

It is evident from Fig. 5 that poly-AA has stronger adsorption in $CaCl_2$ than in KCl. However, the presence of $CaCl_2$ did not prevent the polymer from desorbing from the surface after 2.0 ns. We conclude that the divalent Ca^{2+} cations may enhance the adsorption of poly-AA by slowing its desorption. But from the thermodynamic point of view, KCl and $CaCl_2$ showed no difference at the high temperature (500 K) since the polymer chains eventually desorbed in both cases.

For the other three polymers shown in Fig. 5, adsorption behaviors in KCl have no apparent difference compared with those in $CaCl_2$ solutions at 500 K.

Additional simulations at 275 K provided in Fig. S4† suggest that similar conclusions can be drawn for low temperatures. Only poly-AA is affected by the presence of $CaCl_2$.

Open Access Article. Published on 11 January 2023. Downloaded on 12/19/2025 10:25:52 PM.
This article is licensed under a Creative Commons Attribution-NonCommercial 3.0 Unported Licence.

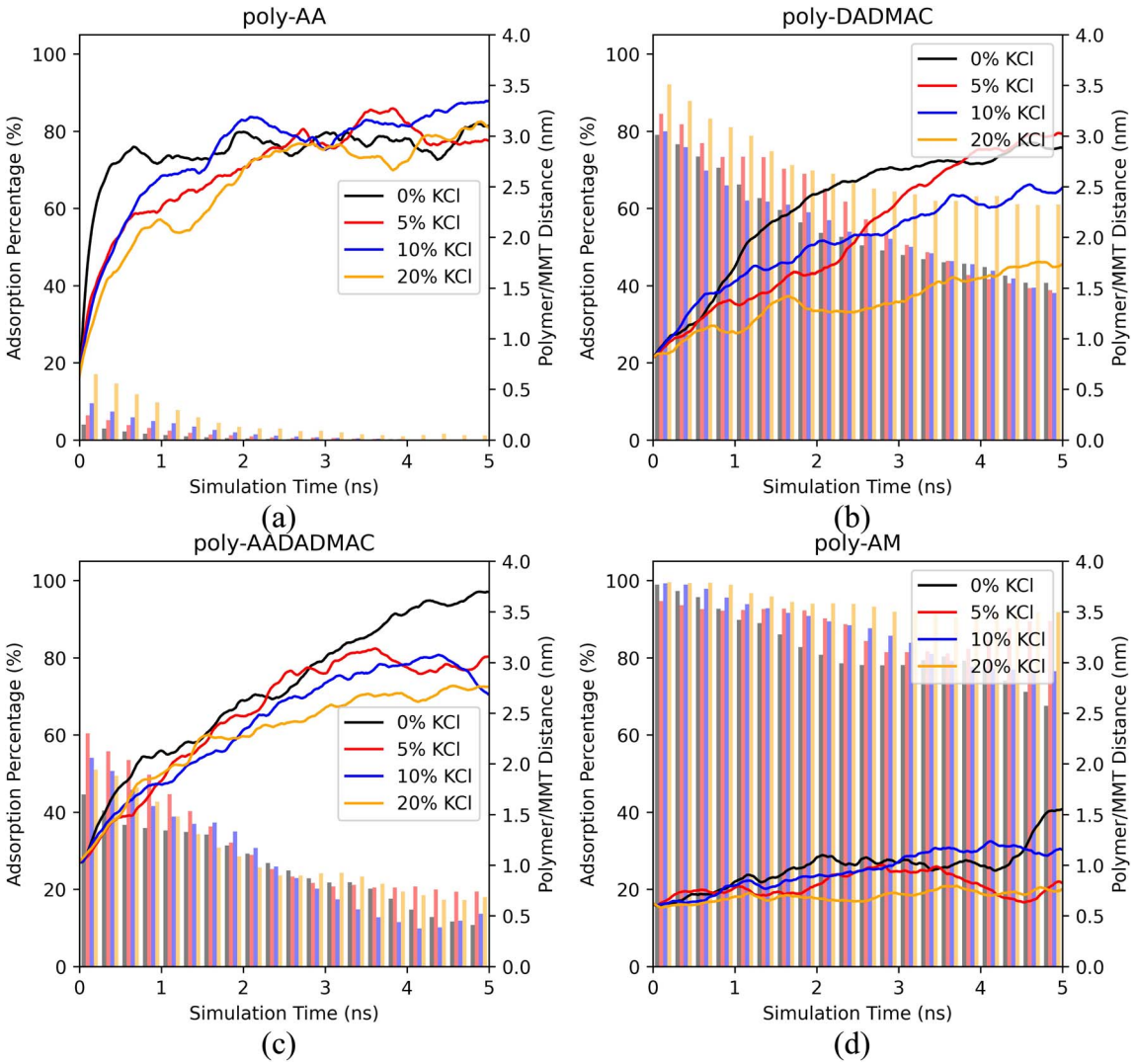

Fig. 4 The polymer/MMT distances and the ratios of adsorbed polymer chains of (a) poly-AA, (b) poly-DADMAC, (c) poly-AADADMAC, and (d) poly-AM as functions of MD simulation time under different KCl concentrations. All simulations were at 500 K, 50 MPa.

3.2 Adsorption mechanisms

3.2.1 Adsorption under low temperatures. From the results in previous sections, it is still not clear what leads to the different desorption kinetics of these four polymers. This section focuses on the adsorption mechanisms of polymers on the MMT surface.

Unfortunately, significant desorption of polymer chains can be observed at or above 300 K. To obtain structures in which polymer chains are adsorbed on the MMT surface, we lowered the temperature to 275 K and performed a series of simulations. These results are summarized in Fig. S3,† which is previously referenced in Section 3.1.3 as a part of the investigation into salinity dependency. At 275 K and in 10% KCl solution, all polymers including poly-AA are on average within 1.5 nm from the MMT surface. Therefore, the subsequent analysis of adsorption mechanisms will be performed based on the results under the 275 K, 10% KCl condition.

We have calculated the distributions of polymer chains and salt ions along the *z*-direction (perpendicular to the MMT surface) averaged over each five-nanosecond trajectory and plotted them in Fig. 6. Positions of characteristic functional groups of each polymer are chosen to represent the locations of polymer chains. Specifically, the distributions of carboxyl groups (COO^-) on poly-AA, tertiary ammonium nitrogen (>N<$^+$) on poly-DADMAC, COO^- and >N<$^+$ on poly-AADADMAC, and amide ($CONH_2$) on poly-AM are shown. Furthermore, for each polymer, Fig. 7 shows the structure of the molecular system after 3.0 ns of MD simulations. These snapshots are intended to provide an intuitive, but less rigorous, representation of the typical structures of adsorbed polymer chains. In addition, radial distribution functions (RDFs) between polymer functional groups and salt ions are shown in Fig. S5.†

Since the carboxyl groups and the MMT surface carry like charges and repel each other, Fig. 6(a) suggests that the carboxyl groups keep a minimum distance of 0.5 nm and are most likely

© 2023 The Author(s). Published by the Royal Society of Chemistry

Open Access Article. Published on 11 January 2023. Downloaded on 12/19/2025 10:25:52 PM.
This article is licensed under a Creative Commons Attribution-NonCommercial 3.0 Unported Licence.

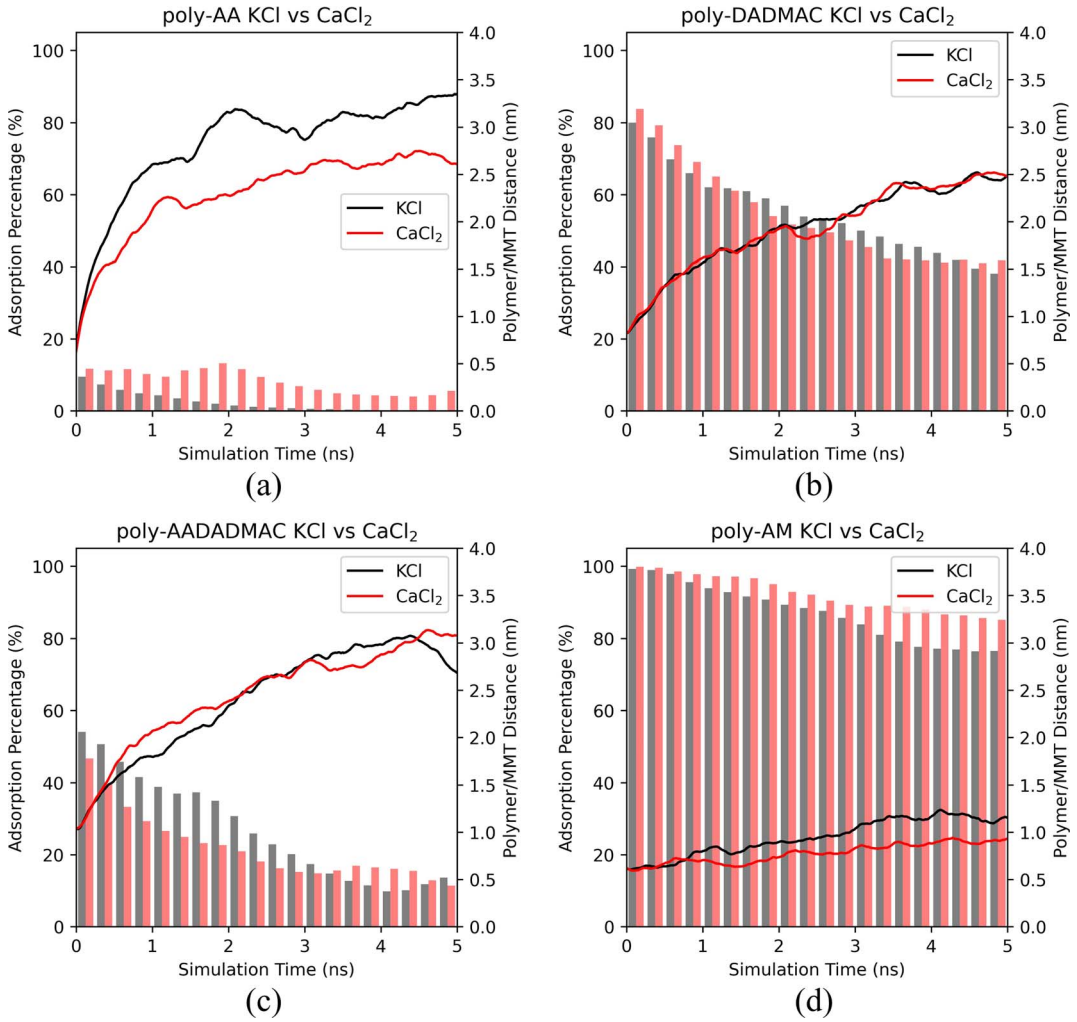

Fig. 5 The polymer/MMT distances and the ratios of adsorbed polymer chains of (a) poly-AA, (b) poly-DADMAC, (c) poly-AADADMAC, and (d) poly-AM as functions of MD simulation time in 10 wt% KCl and 7.54 wt% $CaCl_2$ solutions at 500 K and 50 MPa.

1.2 nm away from the surface. Meanwhile, K^+ aggregate between the polymer and the MMT surface as counter ions to form an electric double-layer (EDL). The interaction between poly-AA and the MMT is dominated by coulombic forces, which rely on the existence of cations between the polymer and the clay. This mechanism can explain the observation that both the existence of divalent Ca^{2+} ions and higher salinity can enhance the adsorption stability because the coulombic forces are proportional to the amounts of charges. On the other hand, under high temperatures (500 K), cations with larger kinetic energies are more likely to escape the polymer/clay interfacial region, which may lead to the desorption of poly-AA.

As shown in Fig. 6(b), positively charged poly-DADMAC is attracted to the negatively charged Na-MMT surface in the adsorbed state. The density of poly-DADMAC splits into three peaks, which can be attributed to DADMAC sidechains that point towards the surface, sideways, and upwards as suggested by the close-up view in Fig. 7(b). The first peak of $>N<^+$ appears at around 0.5 nm, much closer than the most probable 1.2 nm distance between poly-AA and MMT surface. Furthermore, the first peak of $>N<^+$ is followed by a peak of Cl^- at 0.7 nm. The $>N<^+$ groups from poly-DADMAC and Cl^- ions form an EDL similar to poly-AA, which may stabilize the adsorbed polymer chains and can explain why high salinity also favors the adsorption of poly-DADMAC.

The adsorption mechanism of poly-AADADMAC appears to be a combination of poly-DADMAC and poly-AA. As shown in Fig. 6(c), only DADMAC units are directly adsorbed on the surface (first peak at 0.5 nm), while AA units are further away from the surface (most likely at 0.7 nm). Since the polymer chain itself is charge neutral, neither cations nor anions accumulate between the polymer and the clay surface, and the peaks of Cl^- almost coincide with >N<+, and K^+ peaks coincide with COO^- peaks. The DADMAC and AA units form a dipole with positively charged DADMAC units facing the surface. Not surprisingly, the adsorption stability of poly-AADADMAC is stronger than poly-AA but weaker than poly-DADMAC because the adsorption affinity is contributed mainly by the DADMAC units, and poly-AADADMAC is a 1 : 1 copolymer of AA and DADMAC units.

© 2023 The Author(s). Published by the Royal Society of Chemistry

Open Access Article. Published on 11 January 2023. Downloaded on 12/19/2025 10:25:52 PM.
This article is licensed under a Creative Commons Attribution-NonCommercial 3.0 Unported Licence.

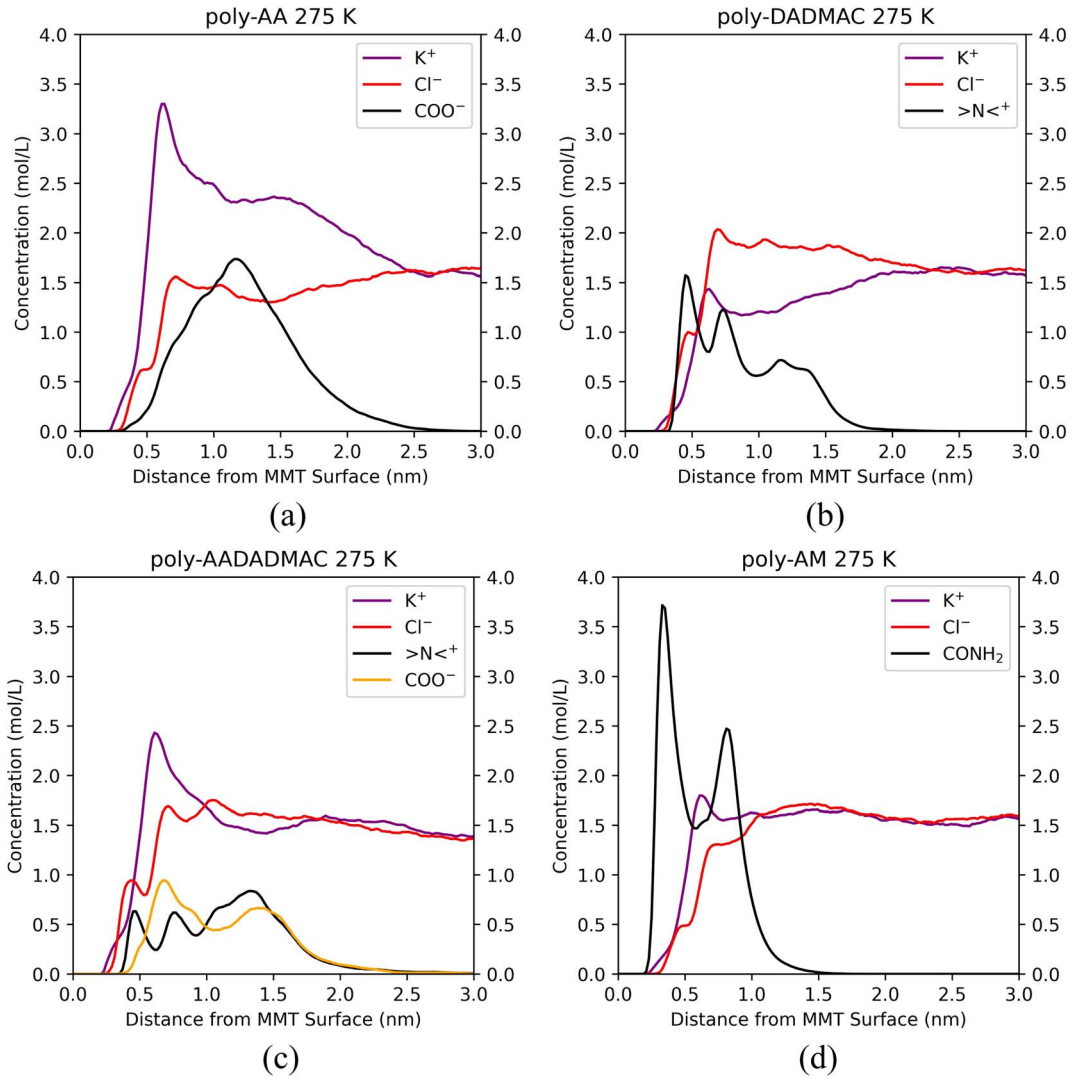

Fig. 6 Distributions of polymer functional groups and salt ions along the z-direction for (a) poly-AA, (b) poly-DADMAC, (c) poly-AADADMAC, and (d) poly-AM adsorbed on the MMT surface at 275 K, 50 MPa, in 10 wt% KCl solution.

The adsorption mechanism of poly-AM is completely different from the others. The sidechains of poly-AM are polar but not ionic. The amide groups carry negative partial charges and are hydrogen-bond donors. As shown in Fig. 6(d), there are two peaks of $CONH_2$ at 0.4 nm and 0.8 nm, which may correspond to functional groups pointing downward and upward, respectively, as demonstrated in Fig. 7(d). This short amide-surface distance (0.4 nm) leads to significant contributions from van der Waals forces.

Moreover, the amide groups form hydrogen bonds with oxygen atoms on the MMT surface. If we consider the criteria to form a hydrogen bond to be H···O distance less than 0.25 nm and N–H···O angle greater than 100°, our calculations found that each poly-AM chain on average forms 1.64 hydrogen bonds with the surface at 275 K. Under higher temperatures, the average numbers of hydrogen bonds per chain are 1.52, 1.02, and 0.78 at 300 K, 400 K, and 500 K, respectively. Since each chain contains 10 amide groups (Table 1), 8% to 16% amide groups have contributions to hydrogen bonding with the surface. Under temperatures below 400 K, each poly-AM chain is anchored to the MMT surface by at least one hydrogen bond, which may be one of the major reasons for the observed strong adsorption affinity shown in Fig. 2(d).

3.2.2 Desorption under high temperatures. Polymer chains gradually desorb from the MMT surface as the temperature rises. Fig. 8 displays the distributions of ions and polymer functional groups under gradually increasing temperatures. The corresponding RDFs of these simulations are provided in Fig. S6.†

The COO^- peak which appears at 1.2 nm at 275 K (Fig. 6(a)) gradually shifts to the right in Fig. 8(a) and becomes broader at higher temperatures, meaning that poly-AA is no longer attracted to the MMT surface and finally dissolves in the solution.

In Fig. 8(b), the second and third peaks of $>N<^+$, which represent DADMAC units pointing sideways and upwards in the

© 2023 The Author(s). Published by the Royal Society of Chemistry

Open Access Article. Published on 11 January 2023. Downloaded on 12/19/2025 10:25:52 PM.
This article is licensed under a Creative Commons Attribution-NonCommercial 3.0 Unported Licence.

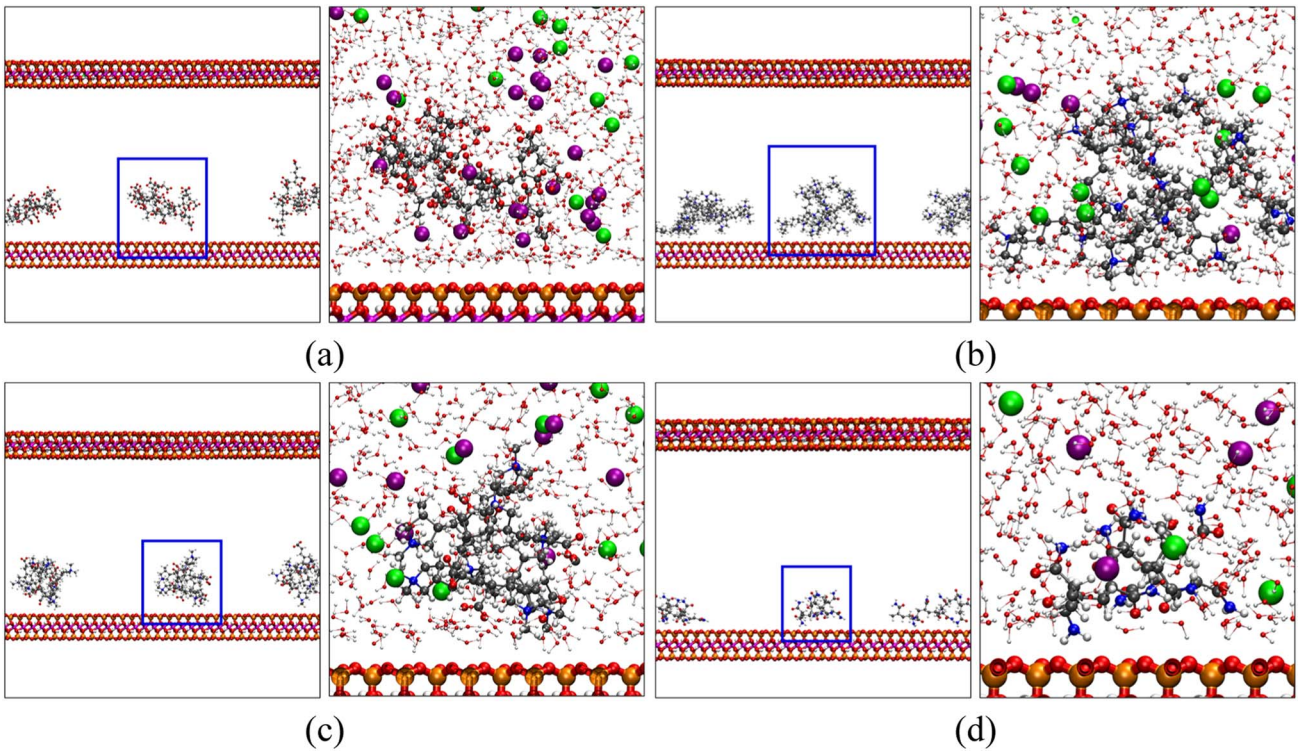

Fig. 7 Snapshots of (a) poly-AA, (b) poly-DADMAC, (c) poly-AADADMAC, and (d) poly-AM adsorbed on the MMT surface after 3.0 ns of MD simulations at 275 K, 50 MPa. In each panel, the figure on the right is a close-up view of the polymer-clay interfacial region highlighted by blue squares on the left. For clarity, water and ions are shown only in the close-up views. In addition to the coloring rules defined in Fig. 1, K^+ and Cl^- are shown as purple and light green spheres, respectively.

original adsorbed poly-DADMAC, gradually flatten out at 400 K and 500 K. However, the first peak at 0.5 nm, which represents $>N<^+$ groups directly attracted to the surface, does not shift or disappear under higher temperatures. Moreover, the area under the first peak is inversely proportional to the temperature (height reduced from around 1.6 mol L^{-1} at 275 K to 0.8 mol L^{-1} at 500 K). These results suggest that the DADMAC units pointing sideways and upwards in the originally adsorbed poly-DADMAC may not have significant contributions to the adsorption stability and can easily detach from the surface, possibly because long-range coulombic forces are screened in solutions with high salinity.

Similarly, Fig. 8(c) indicates that $>N<^+$ peaks can resist the high temperature while the peak of COO^- completely disappears at 500 K. This result corroborates the conclusion that adsorption stability of poly-AADADMAC is mainly contributed by cationic DADMAC units, at least under high temperatures.

Fig. 8(d) further verifies the strong affinity of poly-AM with the MMT surface. The peak at 0.4 nm, which represents amide groups directly attached to the surface *via* hydrogen bonds, does not shift its position under high temperatures. But the second peak gradually disappears. The height of the first peak drops from 3.75 mol L^{-1} at 275 K to 2.1 mol L^{-1} at 500 K, which matches the change in the number of average hydrogen bonds between poly-AM and the surface from 1.64 at 275 K to 0.78 at 500 K.

3.2.3 Insights on enhancing the adsorption stability. Based on the results discussed in the previous sections, the adsorption mechanisms of these four polymers can be conceptually illustrated in Fig. 9.

Fig. 9 summarizes the adsorption mechanisms discovered in this study. Specifically, Fig. 9(a) demonstrates the EDL structure formed by K^+ and COO^- groups on poly-AA. Fig. 9(b) also depicts the EDL by $>N<^+$ and Cl^-. For the neutral poly-AADADMAC, Fig. 9(c) shows that poly-AADADMAC is stabilized on the surface through the contributions from both DADMAC and AA units, and Fig. 9(d) indicates that van der Waals interactions and hydrogen bonds exist between poly-AM and the surface.

Adsorption mechanisms revealed by the simulations can also provide insights into the strategies to enhance the polymer/clay interactions:

(1) Strongly polar polymers should have higher adsorption stability than anionic or cationic polymers under high temperatures (>500 K). The introduction of hydrogen bond donors can enhance the adsorption of polymer on MMT.

(2) Cationic polymers should have stronger adsorption stability than anionic polymers since they can be attracted to the negatively charged clay surface directly through coulombic forces. However, cationic polymers are less stable than neutral polar polymers, especially under high temperatures. A possible strategy to increase the adsorption stability is to introduce both cationic and polar repeating units into the polymer chains.

Open Access Article. Published on 11 January 2023. Downloaded on 12/19/2025 10:25:52 PM.
This article is licensed under a Creative Commons Attribution-NonCommercial 3.0 Unported Licence.

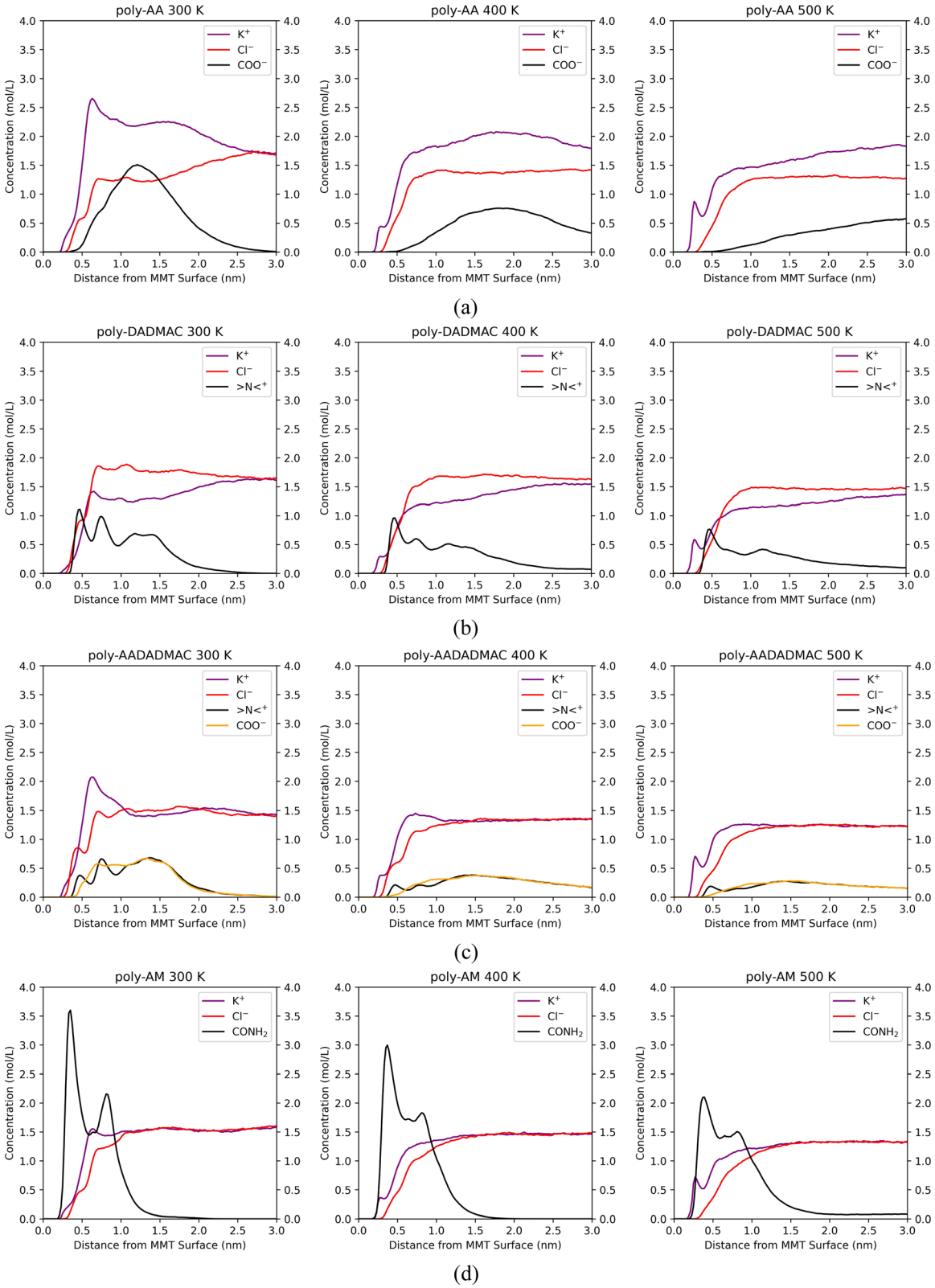

Fig. 8 Distributions of polymer functional groups and salt ions along the z-direction for (a) poly-AA, (b) poly-DADMAC, (c) poly-AADADMAC, and (d) poly-AM at 300 K, 400 K, and 500 K. All simulations in this figure are at 50 MPa, in 10 wt% KCl solution.

(3) High salinity favors the adsorption of both anionic and cationic polymers. A possible reason is that the EDL structure formed under high salinity can better stabilize the adsorbed polymer chains. Charged polymers, especially polymers with cationic units, should be recommended in high-salinity environments.

© 2023 The Author(s). Published by the Royal Society of Chemistry

Open Access Article. Published on 11 January 2023. Downloaded on 12/19/2025 10:25:52 PM.
This article is licensed under a Creative Commons Attribution-NonCommercial 3.0 Unported Licence.

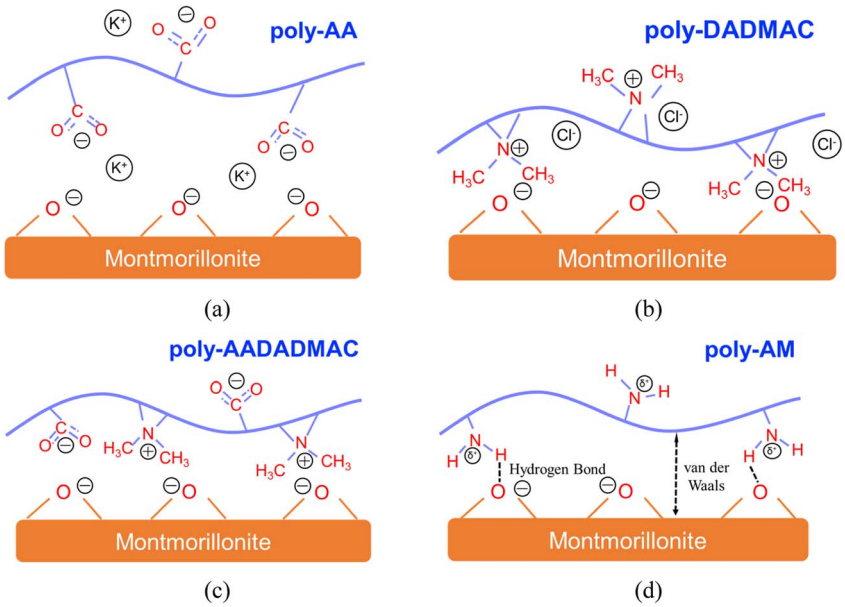

Fig. 9 Illustrations for the adsorption mechanisms of (a) poly-AA, (b) poly-DADMAC, (c) poly-AADADMAC, and (d) poly-AM on MMT surfaces.

4 Conclusion

In this study, we have simulated the desorption kinetics and mechanisms of poly-AA, poly-DADMAC, poly-AADADMAC, and poly-AM from the Na-MMT surface. We found that the adsorption stability follows the order of poly-AM > poly-DADMAC > poly-AADADMAC > poly-AA. This order of relative stability remains the same under different temperatures, pressures, and salinity.

We found that temperature significantly affects the adsorption stability of polymers as all polymers are less stable under higher temperatures. Pressure is only a minor factor of adsorption stability as polymers are marginally more sable under higher pressures. High salinity favors the adsorption of both positively and negatively charged polymers but has negligible influence on neutral polymers.

Based on the simulation results, we predict that a polymer with small and strongly polar sidechains, for example with hydrogen donor sites similar to poly-AM, would adsorb firmly on clay surfaces. Positively charged polymers would also have strong adsorption stability. On the other hand, anionic polymers would have limited adsorption stability on negatively charged clay surfaces under high temperatures.

One limitation of this study is that only montmorillonite was investigated while other types of clay minerals are also widely used in drilling fluids. Furthermore, only the basal planes of clays are considered due to periodic boundary conditions, while in reality, the clay platelet edges may also be adsorption sites. Our future work will be focused on the adsorption of polymers on other types of clay under more complex situations by considering the influence of pH values and platelet edges. Nevertheless, the simulation framework and insights proposed in this study can be extended and utilized in the design and screening of polymers with high adsorption stability on clays, which will also be the aim of our future studies.

Author contributions

Conceptualization, Yuanzhi Qu, Ling Lin, and Wenjia Luo; methodology, Ling Lin; software, Wenjia Luo, Hongjun Huang, and Xin Li; validation, Ling Lin, Yukun Yang, and Ren Han; formal analysis, Hongjun Huang and Ren Han; investigation, Yukun Yang and Xin Li; resources, Yuanzhi Qu and Ling Lin; data curation, Yuanzhi Qu; writing-original draft preparation, Wenjia Luo and Ling Lin; writing-review and editing, Wenjia Luo; visualization, Hongjun Huang and Han Ren; supervision, Ling Lin and Wenjia Luo; project administration, Yuanzhi Qu, Ling Lin, and Wenjia Luo; funding acquisition, Yuanzhi Qu and Ling Lin.

Conflicts of interest

The authors declare no conflict of interest.

Acknowledgements

This work was financially supported by CNPC key core technology project (Environment-friendly new materials for wellbore working fluid with temperature resistance above 240 °C, grant no. 2020A-3913) and the National Natural Science Foundation of China (grant no. 41702391).

References

1 J. S. Essomba, J. P. Alla, P. D. B. Belibi and N. N. Fathima, *Int. J. Environ. Sci. Technol.*, 2022, **19**, 5181–5194.

© 2023 The Author(s). Published by the Royal Society of Chemistry

Open Access Article. Published on 11 January 2023. Downloaded on 12/19/2025 10:25:52 PM.
This article is licensed under a Creative Commons Attribution-NonCommercial 3.0 Unported Licence.

2 Ş. Yılmaz, A. Zengin and T. Şahan, *Colloids Surf., A*, 2021, **612**, 125979.
3 A. Amari, F. Mohammed Alzahrani, K. Mohammedsaleh Katubi, N. Salem Alsaiari, M. A. Tahoon and F. Ben Rebah, *Materials*, 2021, **14**, 1365.
4 E. Baigorria and L. F. Fraceto, *J. Cleaner Prod.*, 2022, **331**, 129867.
5 J. Dong, Z. Cheng, S. Tan and Q. Zhu, *Expert Opin. Drug Delivery*, 2021, **18**, 695–714.
6 N. Khatoon, M. Q. Chu and C. H. Zhou, *J. Mater. Chem. B*, 2020, **8**, 7335–7351.
7 N. Mohamadian, H. Ghorbani, D. A. Wood and M. A. Khoshmardan, *J. Polym. Res.*, 2019, **26**, 33.
8 H. M. Ahmad, M. S. Kamal and M. A. Al-Harthi, *Appl. Clay Sci.*, 2018, **160**, 226–237.
9 X. Jia, X. Zhao, B. Chen, S. B. Egwu and Z. Huang, *Appl. Surf. Sci.*, 2022, **578**, 152089.
10 R. Saboori, S. Sabbaghi and A. Kalantariasl, *Powder Technol.*, 2019, **353**, 257–266.
11 M. A. Abbas, A. Zamir, K. A. Elraies, S. M. Mahmood and M. H. Rasool, *J. Pet. Sci. Eng.*, 2021, **204**, 108745.
12 F. Zhang, J. Sun, Z. Dai, X. Chang, X. Huang, J. Liu, Z. Wang and K. Lv, *J. Polym. Res.*, 2020, **27**, 107.
13 Q. Chu, J. Su and L. Lin, *Appl. Clay Sci.*, 2020, **185**, 105315.
14 X. Shu, L. Wan and M. Duan, *J. Polym. Eng.*, 2018, **38**, 323–331.
15 P. Liu, *Appl. Clay Sci.*, 2007, **38**, 64–76.
16 O. T. Salami and J. Plank, *J. Appl. Polym. Sci.*, 2013, **129**, 2544–2553.
17 Y. Mansoori, A. Akhtarparast, M. Reza Zamanloo, G. Imanzadeh and T. M. Masooleh, *Polym. Compos.*, 2011, **32**, 1225–1234.
18 K. R. Reddy, C. Venkata Reddy, B. Babu, K. Ravindranadh, S. Naveen and A. V. Raghu, in *Modified Clay and Zeolite Nanocomposite Materials*, ed. M. Mercurio, B. Sarkar and A. Langella, Elsevier, 2019, pp. 197–218.
19 M. Abbasian, M. Seyyedi and M. Jaymand, *Polym. Bull.*, 2020, **77**, 1107–1120.
20 A. Vasudeo Rane, K. Kanny, V. K. Abitha, S. S. Patil and S. Thomas, in *Clay-Polymer Nanocomposites*, ed. K. Jlassi, M. M. Chehimi and S. Thomas, Elsevier, 2017, pp. 113–144.
21 H. Lei, J. Lou, X. Li, M. Jiang and C. Tu, *Int. J. Geomech.*, 2020, **20**, 04020050.
22 J. Cao, L. Meng, Y. Yang, Y. Zhu, X. Wang, C. Yao, M. Sun and H. Zhong, *Energy Fuels*, 2017, **31**, 11963–11970.
23 G. Wang, G. Jiang, J. Yang, L. Yang, X. Li, Y. He and X. Chang, *J. Appl. Polym. Sci.*, 2021, **138**, 51001.
24 M. T. Alsaba, M. F. Al Dushaishi and A. K. Abbas, *J. Pet. Explor. Prod. Technol.*, 2020, **10**, 1389–1399.
25 S. Gautam, C. Guria and V. K. Rajak, *J. Pet. Sci. Eng.*, 2022, **213**, 110318.
26 J. Sun, X. Zhang, K. Lv, J. Liu, Z. Xiu, Z. Wang, X. Huang, Y. Bai, J. Wang and J. Jin, *J. Pet. Sci. Eng.*, 2022, **209**, 109808.
27 F. Kádár, L. Százdi, E. Fekete and B. Pukánszky, *Langmuir*, 2006, **22**, 7848–7854.
28 G. Cheraghian, S. S. Khalili Nezhad, M. Kamari, M. Hemmati, M. Masihi and S. Bazgir, *Int. Nano Lett.*, 2014, **4**, 1–8.
29 R. Y. Lochhead and C. M. Boykin, in *Polymer Nanocomposites*, American Chemical Society, 2001, ch. 8, vol. 804, pp. 85–98.
30 A. I. Nakatani, C. E. Mohler and S. Hughes, *Soft Matter*, 2021, **17**, 6848–6862.
31 H. Kohay, I. I. Bilkis and Y. G. Mishael, *J. Colloid Interface Sci.*, 2019, **552**, 517–527.
32 R. J. Sengwa and S. Choudhary, *J. Appl. Polym. Sci.*, 2014, **131**, 40617.
33 S. P. Pereira, G. Scocchi, R. Toth, P. Posocco, D. R. Nieto, S. Pricl and M. Fermeglia, *J. Multiscale Modell.*, 2011, **03**, 151–176.
34 J. L. Suter, L. Kabalan, M. Khader and P. V. Coveney, *Geochim. Cosmochim. Acta*, 2015, **169**, 17–29.
35 R. T. Cygan, J. A. Greathouse, H. Heinz and A. G. Kalinichev, *J. Mater. Chem.*, 2009, **19**, 2470–2481.
36 B. J. Teppen, K. Rasmussen, P. M. Bertsch, D. M. Miller and L. Schäfer, *J. Phys. Chem. B*, 1997, **101**, 1579–1587.
37 M. Camara, J. Xu, X. Wang, J. Zhang, Z. Chen and X. Li, *Appl. Clay Sci.*, 2017, **146**, 206–215.
38 J. A. Greathouse, R. T. Cygan, J. T. Fredrich and G. R. Jerauld, *J. Phys. Chem. C*, 2016, **120**, 1640–1649.
39 R. Shahriyari, A. Khosravi and A. Ahmadzadeh, *Mol. Phys.*, 2013, **111**, 3156–3167.
40 S. Yang, X. Li, Z. Jia, Q. Li and G. Yang, *Soil Sci. Soc. Am. J.*, 2018, **82**, 1384–1391.
41 Y. Zhang, X. Liu, C. Zhang and X. Lu, *Geochim. Cosmochim. Acta*, 2020, **291**, 110–125.
42 A. A. Tsukanov and S. G. Psakhie, *Sci. Rep.*, 2016, **6**, 19986.
43 A. Kadoura, A. K. Narayanan Nair and S. Sun, *J. Phys. Chem. C*, 2016, **120**, 12517–12529.
44 J. A. R. Willemsen, S. C. B. Myneni and I. C. Bourg, *J. Phys. Chem. C*, 2019, **123**, 13624–13636.
45 S. He, J. C. Palmer and G. Qin, *Microporous Mesoporous Mater.*, 2017, **249**, 88–96.
46 Z. Wang, C. Yu, J. Zhao, P. Guo and H. Liu, *J. Mater. Res. Technol.*, 2022, **19**, 4371–4380.
47 C. Yu, J. Zhao, Z. Wang, P. Guo, H. Liu, Z. Su and H. Liao, *J. Mol. Liq.*, 2022, **365**, 120075.
48 Y. Li, S. Han, B. Zhang, H. Tang, J. Han, H. Kang, Y. Zhao and J. Zhu, *Appl. Clay Sci.*, 2022, **216**, 106344.
49 Y. Li, M. Chen, H. Tang, S. Han, H. Song, P. Wang, Y. Zhao and J. Zhu, *ACS Sustainable Chem. Eng.*, 2022, **10**, 6358–6369.
50 Y. Li, M. Chen, C. Liu, H. Song, P. Yuan, B. Zhang, D. Liu and P. Du, *Langmuir*, 2020, **36**, 3323–3335.
51 Y. Li, M. Chen, H. Song, P. Yuan, B. Zhang, D. Liu, H. Zhou and H. Bu, *ACS Earth Space Chem.*, 2020, **4**, 572–582.
52 H. Zhang, J. Cao, H. Duan, H. Luo and X. Liu, *Fuel*, 2022, **310**, 122380.
53 P. A. Klonos, L. Papadopoulos, Z. Terzopoulou, G. Z. Papageorgiou, A. Kyritsis and D. N. Bikiaris, *J. Phys. Chem. B*, 2020, **124**, 7306–7317.
54 D. Karataş, A. Tekin, F. Bahadori and M. S. Çelik, *J. Mater. Chem. B*, 2017, **5**, 8070–8082.

© 2023 The Author(s). Published by the Royal Society of Chemistry

Open Access Article. Published on 11 January 2023. Downloaded on 12/19/2025 10:25:52 PM.
This article is licensed under a Creative Commons Attribution-NonCommercial 3.0 Unported Licence.

55 Y. Wang, J. Wohlert, M. Bergenstråhle-Wohlert, Y. Tu and H. Ågren, *RSC Adv.*, 2015, **5**, 54580–54588.
56 Y. Wang, J. Wohlert, M. Bergenstråhle-Wohlert, J. J. Kochumalayil, L. A. Berglund, Y. Tu and H. Ågren, *Biomacromolecules*, 2015, **16**, 257–265.
57 Y. Wang, J. Wohlert, L. A. Berglund, Y. Tu and H. Ågren, *J. Mater. Chem. A*, 2014, **2**, 9541–9547.
58 M. Krishnan, M. Saharay and R. J. Kirkpatrick, *J. Phys. Chem. C*, 2013, **117**, 20592–20609.
59 J. L. Suter and P. V. Coveney, *Soft Matter*, 2009, **5**, 2239–2251.
60 F. Gardebien, J.-L. Brédas and R. Lazzaroni, *J. Phys. Chem. B*, 2005, **109**, 12287–12296.
61 F. Gardebien, A. Gaudel-Siri, J.-L. Brédas and R. Lazzaroni, *J. Phys. Chem. B*, 2004, **108**, 10678–10686.
62 R. Toth, D.-J. Voorn, J.-W. Handgraaf, J. G. E. M. Fraaije, M. Fermeglia, S. Pricl and P. Posocco, *Macromolecules*, 2009, **42**, 8260–8270.
63 G. R. Quezada, R. E. Rozas and P. G. Toledo, *Miner. Eng.*, 2021, **162**, 106741.
64 A. Jacquet, D. L. Geatches, S. J. Clark and H. C. Greenwell, *Minerals*, 2018, **8**, 130.
65 Q.-X. Pei, V. Sorkin, P. Liu, Y. Zhong, W. Thitsartarn, C. He and Y.-W. Zhang, *J. Polym. Res.*, 2021, **28**, 29.
66 L. Kabalan, M. M. Zagho, M. J. Al-Marri and M. M. Khader, *J. Vinyl Addit. Technol.*, 2019, **25**, 172–181.
67 W. Xu, X. Wu and W. Sun, *Adv. Mech. Eng.*, 2016, **8**, 1–8.
68 K. Hagita, Y. Shudo and M. Shibayama, *Polymer*, 2018, **154**, 62–79.
69 Y. Yang, S. Adhikari and G. Xu, *Surf. Interface Anal.*, 2020, **52**, 665–675.
70 D. Xu, D. Bhatnagar, D. Gersappe, J. C. Sokolov, M. H. Rafailovich and J. Lombardi, *Macromolecules*, 2015, **48**, 840–846.
71 V.-H. Nguyen, S. Mahouche-Chergui, B. Carbonnier, D. Di Tommaso and S. Naili, *Comput. Mater. Sci.*, 2017, **139**, 191–201.
72 K. Anoukou, A. Zaoui, F. Zaïri, M. Naït-Abdelaziz and J.-M. Gloaguen, *Phys. E*, 2015, **65**, 56–60.
73 W. Sun, H. Zeng and T. Tang, *J. Phys. Chem. A*, 2021, **125**, 1025–1035.
74 W. Sun, H. Zeng and T. Tang, *Appl. Clay Sci.*, 2020, **193**, 105654.
75 T. Jamil, J. R. Gissinger, A. Garley, N. Saikia, A. K. Upadhyay and H. Heinz, *Nanoscale*, 2019, **11**, 11183–11194.
76 R. El Haouti, H. Ouachtak, A. El Guerdaoui, A. Amedlous, E. Amaterz, R. Haounati, A. A. Addi, F. Akbal, N. El Alem and M. L. Taha, *J. Mol. Liq.*, 2019, **290**, 111139.
77 P. Mpofu, J. Addai-Mensah and J. Ralston, *J. Colloid Interface Sci.*, 2004, **271**(1), 145–156.
78 N. Tekin, A. Dinçer, Ö. Demirbaş and M. Alkan, *J. Hazard. Mater.*, 2006, **134**, 211–219.
79 R. T. Cygan, J.-J. Liang and A. G. Kalinichev, *J. Phys. Chem. B*, 2004, **108**, 1255–1266.
80 A. Viani, A. F. Gualtieri and G. Artioli, *Am. Mineral.*, 2002, **87**, 966–975.
81 S. Plimpton, *J. Comput. Phys.*, 1995, **117**, 1–19.
82 W. L. Jorgensen, D. S. Maxwell and J. Tirado-Rives, *J. Am. Chem. Soc.*, 1996, **118**, 11225–11236.
83 H. J. C. Berendsen, J. R. Grigera and T. P. Straatsma, *J. Phys. Chem.*, 1987, **91**, 6269–6271.
84 R. W. Hockney and J. W. Eastwood, *Computer simulation using particles*, CRC Press, 1988.
85 W. Hoover, *Phys. Rev. A*, 1985, **31**, 1695.

© 2023 The Author(s). Published by the Royal Society of Chemistry